npj | digital medicine

Article

Published in partnership with Seoul National University Bundang Hospital

https://doi.org/10.1038/s41746-026-03056-9

A flexible wearable system for integrated sweat stimulation and chloride analysis in cystic fibrosis diagnosis

Check for updates

Mingyu Zhou[1,2,22], Da Som Yang[3,22], Joohee Kim[4,22], Jae-Hwan Kim[1,5], Evangelos E. Kanatzidis[1], Jong Uk Kim[1,6], Seyong Oh[7], Larissa Rugg[8], Shupeng Li[9], Seungyeob Kim[1,10], Jiheon Kang[1], Hanbang Hua[1], Jihun Park[1], Tonglu Zhou[1,2], Chanho Park[11], Seung Gi Seo[1], Young Jin Jo[1], Jihun Cha[1,12], Jiwon Kim[13], Alexander J. Aranyosi[1,14], Yonggang Huang[1,9], Manu Jain[15,16,17,18], Roozbeh Ghaffari[1,2,14], Susanna A. McColley[8,19] ✉ & John A. Rogers[1,2,20,21] ✉

Cystic Fibrosis (CF) diagnosis relies on quantitative sweat chloride testing, a process that requires highly trained personnel, bulky instrumentation, and a cumbersome workflow performed at specialized clinical centers with high per-test cost. Recent advances in wearable sweat biomarker sensors offer opportunities for the development of point-of-care CF sweat chloride analysis. This work presents a flexible, wearable platform for sweat chloride testing, based on miniaturized, automated iontophoresis stimulation, microfluidic sweat collection, and colorimetric chloride analysis. This system enables quantitative, visually interpretable chloride measurements without external instrumentation, requires only microliters of sweat to operate, and reduces the per-test cost to around 1 dollar. Clinical evaluation of the device with 55 subjects at a single pediatric CF center demonstrates strong agreement between chloride concentrations from standard-of-care sweat testing and this platform, with reliable operation across physiologically relevant chloride concentrations. This platform provides a practical, scalable alternative for CF diagnosis in a range of clinical settings with potential for use in the home.

Wearable biosensors have emerged as powerful tools for health assessments, including non-invasive biochemical analysis of body fluids[1–3]. Sweat analytes offer unique advantages for disease screening, diagnosis, and health monitoring due to their non-invasive accessibility and the minimal discomfort associated with collection[4–6]. Conformal, soft microfluidic designs combined with colorimetric sensing approaches enable microliter-scale sweat capture and visual readouts that can be interpreted with smartphones in real time, without bulky instrumentation, their associated costs, and operational complexity[7–11].

The most established, clinically important applications of sweat analysis are for cystic fibrosis (CF) diagnosis. Since the mid-20th century, pilocarpine iontophoresis followed by sweat collection and quantitative measurement has served as the diagnostic gold standard[12,13], with concentrations above 60 mmol/L (mM) indicating CF[14]. Sweat chloride testing, following guidelines established by the Clinical and Laboratory Standards Institute[14], is recommended for CF diagnosis even when two disease-causing variants of the cystic fibrosis transmembrane conductance regulator (CFTR) gene are confirmed in an individual undergoing diagnostic evaluation[15]. The Gibson–Cooke protocol[12] was standardized in the 1980s with the development of the Macroduct™ Sweat Collection System (Eli-Techgroup Inc.), is in widespread use, and is endorsed by the Cystic Fibrosis Foundation[14,16]. This system uses wired electrodes, external power, hydrogel disks containing pilocarpine, and a coiled collector. Sweat from coils passes manually with a syringe to a small Eppendorf tube for a benchtop chloridometer analysis, which requires a minimum volume of 15–20 μL. Beyond diagnosis, sweat chloride concentration is an important pharmacodynamic measurement for CF clinical trials, particularly for evaluating the efficacy of CFTR modulators[17]. Reductions in sweat chloride concentration are widely accepted as evidence of improved CFTR function to assess therapeutic response and have a potential role in personalized dose optimization[18,19]. Accordingly, sweat chloride concentration has transitioned from a screening/diagnostic biomarker to a key endpoint guiding CF drug development and management[20].

Existing sweat chloride testing procedures have limitations that restrict use and availability. The setup requires electrical wiring, external power supplies, and bulky gel electrodes, as well as specialized equipment and

A full list of affiliations appears at the end of the paper. ✉e-mail: SMcColley@luriechildrens.org; jrogers@northwestern.edu

highly skilled technicians. These factors contribute to delays, increased costs, and limited access outside of centralized clinical centers. The rigid sweat collection vehicle and its pressure seal can be uncomfortable, particularly for infants and pediatric patients. Leakage at the collector-skin interface and inefficient transfer from the coiled tube to the chloridometer may yield inadequate volumes. This leakage can lead to "quantity not sufficient" (QNS) test results and repeated testing[21]. QNS is especially common in young infants. One study reported that approximately 30% of CF centers had mean QNS rates exceeding 10% in infants 14 days old or younger[21]; another documented QNS rates as high as 38% in newborns under one month of age[22]. Resulting repeated testing can delay diagnosis and treatment, with significant clinical impact and burden on patients, families, and clinical systems. Recently developed approaches such as the Nanoduct Neonatal Sweat Analysis System and a proof-of-concept device[23] lower the sample volume requirements but rely on the electrical conductivity of sweat rather than the chloride concentration and therefore lack diagnostic specificity[24,25], limiting clinical adoption.

High costs, QNS testing outcomes, and limited access to sweat testing have a disproportionate impact on underserved populations and those living far from accredited CF centers[26,27]. In the United States, many infants with positive CF newborn screens receive confirmatory testing later than the three working days recommended by the Cystic Fibrosis Foundation[28,29]. Delayed diagnosis is associated with early and sustained nutritional compromise, higher risks of pulmonary exacerbations in the first year of life, and worse long-term pulmonary function and survival[30–32]. Quantitative sweat chloride testing is largely unavailable in many low- and middle-income countries (LMICs), so population CF prevalence is often unknown[33]. In regions that have implemented diagnostic and treatment services, such as South India, high morbidity and mortality have been reported[34], prompting calls for newborn screening that necessitates widespread access to sweat testing[35].

Collectively, these challenges highlight the need for a low-cost point-of-care platform for quantitative sweat chloride analysis without reliance on centralized clinical infrastructure. Recent proof-of-concept work has demonstrated a miniaturized wearable device that integrates pilocarpine iontophoresis, soft sweat microfluidics, and colorimetric analysis with initial validation in small cohorts[36,37]. This report demonstrates expanded clinical studies using an advanced version of this platform called the CF SWIFT (Cystic Fibrosis Sweat Wearable Iontophoretic Field Test) system. This system features an improved miniaturized stimulator with automated electronics and a microfluidic analyzer optimized for precise colorimetric chloride sensing. Validation in 55 subjects demonstrates strong agreement with the Macroduct reference system and represents the largest clinical validation of a wearable sweat chloride platform for CF screening and disease management. These findings support the CF SWIFT system as a highly miniaturized, standalone, and accessible method for CF diagnosis and management.

Results

CF SWIFT: a miniaturized, flexible skin-interfaced CF diagnostic platform

The CF SWIFT system comprises two modules: (i) a miniaturized, flexible electronic stimulator that delivers pilocarpine through the skin by iontophoresis to locally induce sweating (Fig. 1a) and (ii) a soft, flexible sweat analyzer that uses microfluidic channels, reservoirs and chemical reagents to enable colorimetric measurement of sweat chloride concentration (Fig. 1b). Figure 1c, d present images of the circuit and the microfluidic system.

The first step in the use of this system involves mounting the stimulation module onto the arm via a medical-grade adhesive, with pilocarpine-loaded hydrogels in contact with the skin on one side and a pair of electrodes on the other. The stimulator includes a flexible printed circuit board (fPCB; ~100 mm) with a collection of surface-mounted electronic components under a soft, flexible silicone-based encapsulation structure (Fig. 1c). Figure 1e presents a block diagram of the circuit design, powered by a small lithium-polymer battery (3.7 V, 30 mAh). An integrated-circuit regulator (NCP114) supplies a stable 3.3 V to a bluetooth low energy (BLE) chip (ISP1807) that activates the system for a stimulation period of 5 min (Supplementary Fig. 1), defined by firmware programming (Supplementary Fig. 2). Briefly, once the device is turned on manually, the firmware executes activation of stimulation for a programmable duration (default 300 s, selectable in firmware from 0.1 s to 600 s). Stimulation occurs under firmware control using a three-phase schedule (PreStim, T_stim on, PostStim) with T_stim = 300 s (Supplementary Fig. 2). A small, red LED serves as a visual indicator of operation. A low-dropout voltage regulator (TPS7A0318DBVR, Texas Instruments) provides a stable 1.8 V supply that feeds a DC/DC converter (R1218) to deliver 0.25 mA to the anode. A current-limiting resistor limits output to 0.25 mA, below the 4-5 mA range in the clinical CF sweat testing standard CLSI C34[14] and the 1.5 mA typical for the Macroduct Advanced system (2.34 μA/mm² over 641.3 mm²).

The complete circuit schematic is shown in Supplementary Fig. 3. As compared with the previous version[36], the CF SWIFT design uses not only the current-limiting hardware but also programmable, automatic deactivation after 5 min to maintain energy delivery within ranges used for clinical iontophoresis (e.g., Macroduct) and to reduce the risk of skin irritation or electrical injury (Supplementary Table 1). Single-fault condition testing of critical components confirmed safe behavior under fault conditions (Supplementary Note 1). The CF SWIFT stimulation area yields a current density of 1.85 μA/mm² at the skin. Supplementary Fig. 4 demonstrates the simulated current-density distribution (J, mA·cm^{-2}) during 0.25 mA pilocarpine iontophoresis with skin. For power consumption, the stimulation system operates with an average current consumption of 0.09 μA in sleep mode and 11.20 mA during active iontophoresis stimulation at 4.0 V (Supplementary Fig. 5). Using a 30 mAh LiPo battery, the device can support approximately 30 stimulation sessions. Benchtop testing verifies the capability for 27 consecutive stimulation cycles (Supplementary Fig. 6). AC measurements during stimulation reveal a negligible residual AC component (12.6 ± 2.1 μA; ~5% of the 250 μA DC target), detectable for only ~4 s of the 300 s stimulation period (1.3% of total stimulation duration), demonstrating that the current delivered by this device is DC in character (Supplementary Fig. 7 and Supplementary Table 2). The hydrogel elements (3 mm in height, with lateral dimensions that match the areas of the electrodes, 13.5 × 10 mm) use 4 wt% agarose with pH buffer and contain 0.5 wt % pilocarpine. The overall size of the system is 60 × 28 × 7.5 mm, with a weight of 3.3 ± 0.0093 g for the stimulator and 0.76 ± 0.0036 g for the two hydrogels.

Aggravated benchtop cyclic protocols (5% tensile strain at 4 mm·s^{-1} with ±30° articulation at 15°·s^{-1} for 10,000 cycles per device) exceed typical forearm wear[38,39]. Predefined electrical checks in five stimulation modules show no functional failure nor statistically significant change in 5-min stimulation output current after cycling (paired t-test, all $p > 0.05$; maximum mean decrease 0.15%), indicating stable electromechanical performance of the circuit (Supplementary Table 3). Complementary FEA simulations indicate that the circuit is mechanically stable under 15% stretch, 50 mm-radius bending, and 90° twist (Supplementary Fig. 8).

Following ~5 min of constant-current stimulation, removal of the stimulator allows for placement of the microfluidic inlets of the analyzer near the anode location to capture emerging sweat (Fig. 1d). Cleaning the skin with an alcohol wipe and water immediately before placement of the analyzer minimizes contamination from skin surface residues or residual water added during stimulation. Before each application, inspection of the medical-grade adhesive ensured integrity and avoided contamination. After placement, visual inspection verified full contact of the device with skin, by confirming there was no edge lifting or air gaps. Glands activated by pilocarpine push sweat through the circular inlet regions (1-mm diameter), into the microfluidic channels, and finally into reservoir locations containing silver chloranilate, a chemical that reacts with chloride ions in sweat to produce a purple chloranilate dianion in solution (Fig. 1f).

The microfluidic structure uses molded features formed in elastomer poly(dimethylsiloxane) (PDMS) to define the collection channels (depth of 200 mm × width of 200 mm), capillary bursting valves (CBVs; depth of

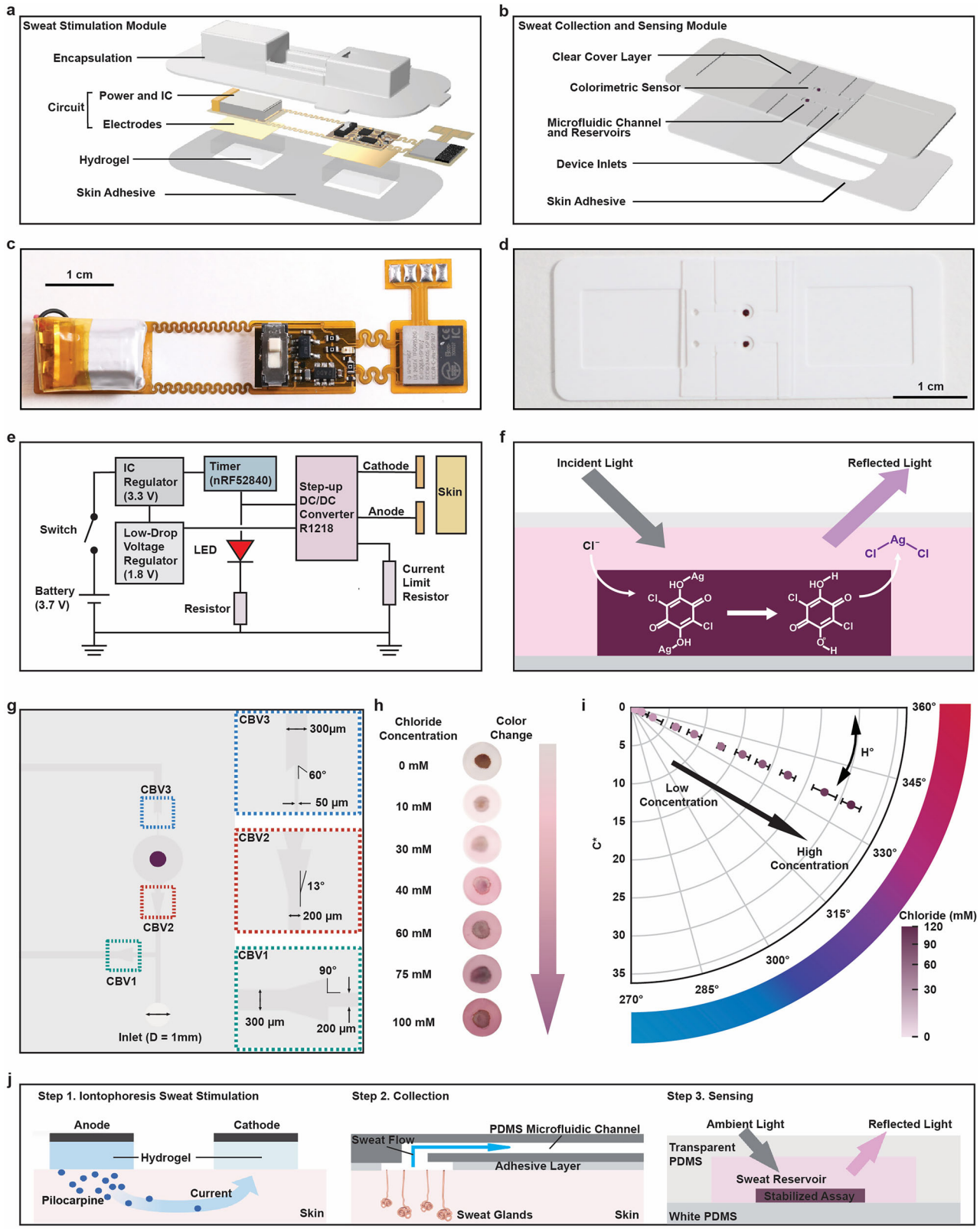


Fig. 1 | Wearable CF SWIFT platform. a Exploded view of the stimulation module. **b** Exploded view of the collection module. **c** Image of the stimulation circuit. **d** Image of the collection patch. **e** Circuit block diagram of the stimulation module. **f** Mechanism and chemical reaction of the colorimetric chloride sensor in the reservoir. **g** Zoomed-in schematic illustration of sampling inlet, reservoir, and CBVs with different channel widths and diverging angles. **h** Images of the reservoir at different levels of chloride concentration. **i** Chroma value (C*) and hue angles (H°) of different chloride concentrations. **j** Mechanism schematic of the platform.

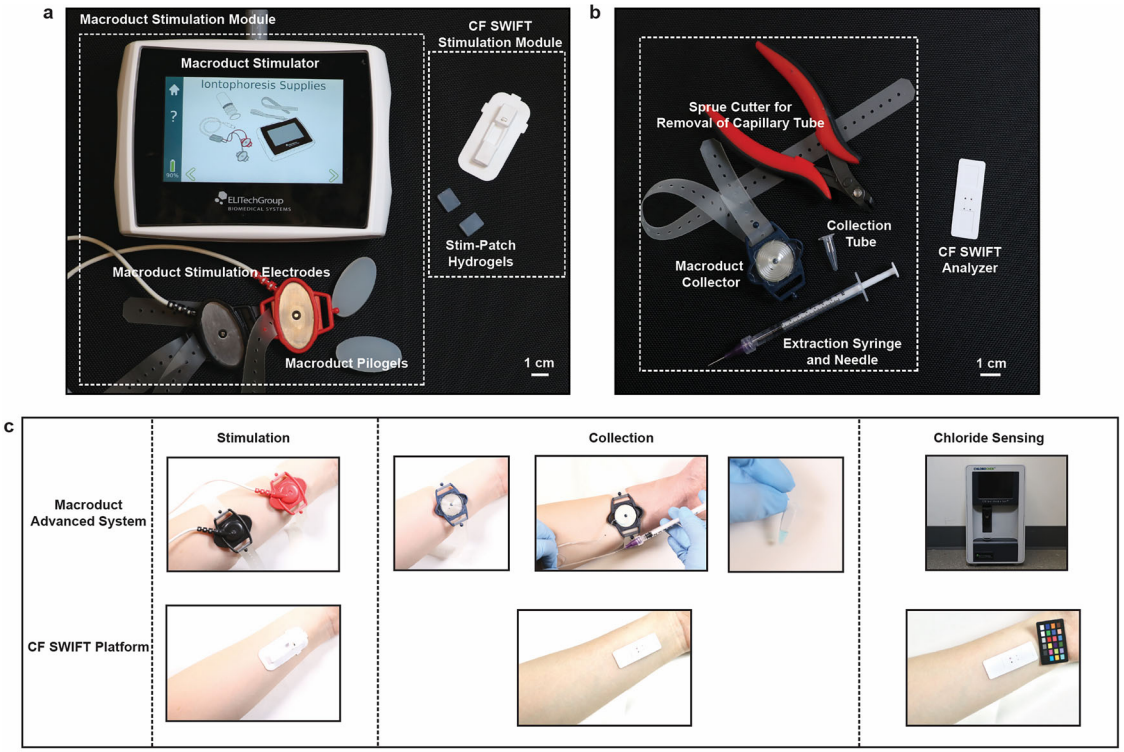


Fig. 2 | Comparison of setup and protocols between the Macroduct Advanced System and the CF SWIFT platform, highlighting the soft, miniaturized, simplified form factor and integrated collection-and-analysis workflow of CF SWIFT. a Image of the stimulation unit for the Macroduct Advanced System and the CF SWIFT platform, along with the hydrogels used. **b** Image of the collection module and other supplies for the Macroduct system and the collection patch for the SWIFT system. **c** Visualization of the workflow of using the SWIFT platform for CF sweat chloride level testing, as compared to the Macroduct Advanced System".

200 μm with varying width), and reservoirs (circular, with depths of 200 mm and diameters of 2 mm), as described previously[36] and shown in Fig. 1g. The bursting pressures of CBV #1, #2, and #3 are 0.4, 0.8, and 12 kPa[36]. As sweat arrives at CBV1 and CBV2, CBV2 bursts first, thereby guiding the flow of sweat into the corresponding reservoir. Once sweat fills this reservoir, excessive sweat passes through CBV1, which has a lower bursting pressure than CBV3, to prevent sweat that initially entered the reservoirs from leaving before completion of the colorimetric reaction. The bursting pressure of CBV3 is significantly higher than the others, to act mainly as an air outlet to relieve back pressure induced by flow of sweat into the system. The use of two reservoirs provides redundancy and allows uncertainty to be quantified from replicate measurements. Each reservoir requires 1.5 μL of sweat, including 0.3 μL to fill the adhesive opening and the microfluidic channels and 1.2 μL for the reservoir itself, more than a factor of ten less volume than that required for standard clinical analysis using the Macroduct system. Equally important, the sweat analysis occurs in situ, without the need for removal from the reservoir. The overall size of the analyzer is 49 × 18 mm, its thickness is 0.70 ± 0.028 mm at its thickest region, and the total weight is 0.45 ± 0.0033 g.

After a 40-min period to account for sweat collection and for reaction with chloranilate, capturing a digital image of the device allows for quantitative extraction of color coordinates to determine the chloride concentration (Fig. 1h and Supplementary Fig. 9). The color extraction algorithm auto-balances the color of the image by using a standard (ColorChecker) placed next to the image as a reference. This scheme minimizes the effects of light temperature and intensity. The algorithm captures six regions of interest (ROI) in each reservoir and extracts the mean L, A, B values in the CIELAB color space. The chloride concentration in each reservoir follows from a calibration curve that connects chloride concentration to chroma value (Fig. 1i, Supplementary Fig. 10a, b), calculated as the distance between the color value in the A–B plane and the origin. Benchtop validation against Inductively Coupled Plasma Optical Emission Spectroscopy (ICP-OES) showed close agreement of SWIFT-derived chloride measurements with the laboratory reference, with minimal mean bias (0.016 mM) and narrow limits of agreement (LoA) (95% LoA from −1.89 to 1.92 mM), supporting the analytical accuracy of the platform under controlled conditions (Supplementary Fig. 10c, d). Unlike previous reports, which relied on the L value[36,37] or CIELAB single pixel values[40], the approach here exploits the chroma value, which tracks the saturation of the colors with a fixed hue angle within the A–B plane. This scheme eliminates the effect of lightness, scattering, and glare, each of which can affect the L values. Colorimetric readouts did not differ significantly across lighting conditions or equipment used for image capture (digital camera or smartphone) for the same analyzer patch, as demonstrated in previous studies of the same colorimetric readout algorithm and in Supplementary Fig. 11. Averaging the reservoir chloride concentrations from the ROIs on the device yields final results and uncertainty estimates, presented in the following. Figure 1i demonstrates the relationship between the chroma value (C*) and hue angle (H°) and concentrations of chloride in the sweat collected in the reservoirs. Figure 1j depicts the mechanisms of sweat stimulation, collection, and colorimetric sensing.

Figure 2 compares the Macroduct Advanced System and the CF SWIFT platform, illustrating the added value of the latter: a flexible, miniaturized form factor and an integrated, simplified collection-and-analysis workflow that eliminates sample transfer and benchtop instrumentation. Figure 2a presents an image of the stimulation module and wired electrodes of the Macroduct system, along with the stimulator of the system presented here. Figure 2b compares the microfluidic/colorimetric analyzer to the collector module of the Macroduct system, the sprue cutter used for the removal of the capillary tube, the syringe and 21 Gauge needle for the removal of sweat, and the tube for storage and transport of the collected sweat for chloride analysis using the Macroduct Chlorochek. The chloride testing workflows of the Macroduct system and the CF SWIFT technology reported here are as illustrated in Fig. 2c.

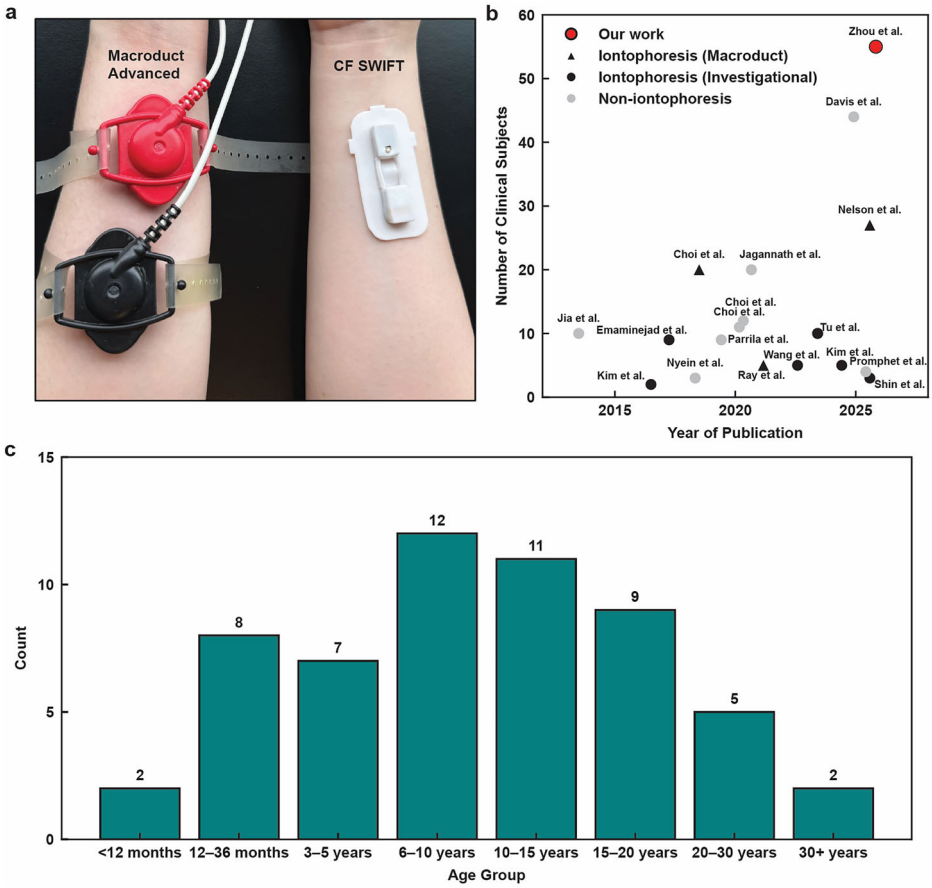


Fig. 3 | Clinical comparison study between the CF SWIFT platform and the Macroduct system. **a** Image of study testing setup, with Macroduct Advanced stimulator placed on one arm and the CF SWIFT stimulator on the other. **b** Clinical sample size scatter benchmark figure of wearable sweat sensors. **c** Age distribution of the study cohort.

Clinical study design

The study was an observational single-center study conducted at Ann & Robert H. Lurie Children's Hospital of Chicago. Eligible participants included healthy adults (over 18 years of age) and children and young adults (age 14 days to 21 years) diagnosed with CF, diagnosed in accordance with CF Foundational Clinical Practice guidelines[14], or CFTR-related metabolic syndrome (CRMS, also called CF Screen Positive, Inconclusive Diagnosis)[41]. The study intentionally recruited participants with an expected broad range of sweat chloride values: those with CF and not on a CFTR modulator therapy, expected to have sweat chlorides > 60 mmol/L; those on modulator therapy, who frequently have intermediate (30–59 mmol/L) or normal (<30 mmol/L) sweat test results, and those with CRMS, expected to have intermediate sweat test results. Participants with inflammation, rash, or other dermatologic conditions, or any other contraindications for sweat testing in accordance with Clinical and Laboratory Science Institute guidelines[14] for sweat testing were excluded. Adults (>18 years old) or parents/legal guardians of children (<18 years old) provided written, informed consent, and children ≥12 years old provided written or verbal assent. Each participant had sweat collected from one arm, and chloride concentrations were analyzed using the Macroduct system and had sweat stimulated and collected using the CF SWIFT system at a similar location on the contralateral arm (Fig. 3a). The primary outcome measure was the correlation between the Macroduct system and CF SWIFT-measured chloride concentrations. The study was approved by the Lurie Children's Hospital Institutional Review Board (IRB00000248).

Table 1 summarizes the demographics and CF-related diagnostic categories of 55 participants (Fig. 3b and Supplementary Table 4 compare the scope of other studies). Forty-two had CF (76.4%), 10 had CRMS (18.2%), and 3 were healthy controls (5.5%). Among those with CF, 47.6% (20 out of 42) were taking CFTR modulator therapy. Overall, 17.9% of participants were younger than 36 months of age, and 87.5% were younger than 20 years (Fig. 3c). No participant (0 out of 55) had a QNS sweat collection in this cohort. No adverse events related to electrical stimulation or device application were reported.

Device validation: agreement between macroduct and CF SWIFT

Figure 4a plots the chloride concentrations determined with the Macroduct system and with the technology introduced here, highlighting the excellent agreement (Pearson's correlation coefficient, 0.98). Diagnostic category was based on the participant's diagnosis prior to participation. The Bland–Altman plot in Fig. 4b demonstrates the difference between the two methods with respect to the mean of the paired measurements. The black dashed line represents the bias of 0.43 mM, and the red dashed lines represent LoA of 0.43 ± 12 mM. As illustrated in Fig. 4c, 84% of paired measurements differ by less than 10 mM. No values exhibit differences larger than 15 mM. The mean signed and absolute differences are 0.45 mM and 5.4 mM, respectively.

Further analysis compares the outlier rate (>10 mM) in data collected with the system reported here with that reported by LeGrys et al.[42], as shown in Supplementary Table 5. In the LeGrys study, differences in sweat chloride concentration between the left and right arms of the same subject, collected simultaneously, quantify physiological variability. Assuming normally distributed paired differences, the data from the LeGrys study suggest an outlier rate (i.e., proportion of paired differences > 10 mM), of ~10%, consistent with the outlier frequency for the data reported here, at the $\alpha = 0.05$ level ($p = 0.17$). Mean bias (0.45 mM vs 0.50 mM), SD (6.5 vs 5.7 mM), and LoA (±12 vs ±11 mM) were similar between the two studies. In additional bilateral testing in healthy subjects using the present system (Fig. 4e), mean absolute and signed differences between right and left arms were +4.3 mM (SD = 2.6 mM, SEM = 0.87 mM, 95% CI = 2.3–6.3 mM) and 1.46 mM (Right–Left). A paired t-test showed no statistically significant difference between arms ($t = 0.87$, $p = 0.41$).

Table 1 | Demographics summary of the enrolled cohort

Section	Level	Healthy ($n = 3$)	CRMS ($n = 10$)	CF with modulators ($n = 20$)	CF without modulators ($n = 22$)
Age	<12 months	0	1	0	1
	12–36 months	0	2	2	4
	3–10 years	0	3	5	10
	10–20 years	0	4	11	5
	20–30 years	1	0	2	2
	30+ years	2	0	0	0
Gender	F	2	7	9	5
	M	1	3	11	17
Race	Asian	1	0	0	3
	Black	0	0	1	1
	Other	1	3	6	4
	White	1	7	12	13
	Not reported	0	0	1	1
Ethnicity	Hispanic or Latino	1	3	7	4
	Not Hispanic or Latino	2	7	13	16
	Not reported	0	0	0	2
Modulator	Ivacaftor	0	0	2	0
	Lumacaftor–Ivacaftor	0	0	2	0
	Tezacaftor–Ivacaftor	0	0	2	0
	Elexacaftor–Tezacaftor–Ivacaftor	0	0	14	0

Evaluations of device analytical concordance follow CLSI guidelines that define acceptable analytical concordance between duplicate sweat collections as a difference of ≤10 mM for values below 60 mM and ≤15 mM for values at or above 60 mM[14,43,44]. Concordance between the CF SWIFT device and the Macroduct system relies on these criteria across 55 paired measurements (Supplementary Table 6). CF SWIFT demonstrates concordance with Macroduct in 50 of 55 measurements (90.9%). Concordance is 100% (25/25) in the ≥60 mM stratum, and 83.3% in both the <30 mM (10/12) and 30–59 mM (15/18) strata, which represent sweat chloride diagnostic categories (CF likely, CF unlikely, and CF possible, respectively). Of the five discordant measurements, four involve values that remain within the same diagnostic category on both devices—that is, neither device produces a result that would alter clinical interpretation—but exceed the ≤10 mM numerical threshold by a margin of 0.3–1.6 mM. In terms of categorical stratum assignment alone, 51 of 55 measurements (92.7%) are classified identically by both devices, with all four categorically discordant cases involving values within 15 mM of a stratum boundary.

Per CLSI guidelines, Macroduct sweat chloride testing is performed bilaterally, with results from two independent arm collections; the inherent physiological and analytical variability between arms is accepted as part of routine clinical practice. This study shows 90.9% concordance overall, and 100% concordance in the ≥60 mM stratum, as achieved from a single paired collection per device.

Subgroup analysis: performance across diagnostic and treatment groups

Figure 5 presents grouped paired box/point plots with accompanying summary statistics, showing paired measurements from subjects using these two systems across diagnostic and treatment groups. CF participants without modulators exhibit the highest absolute chloride levels (Macroduct mean ≈ 89 mM), followed by CF with modulators (≈52 mM), CRMS (mid-30s mM), and healthy controls (low 20 s mM), consistent with levels expected for these populations. This gradient reflects the expected physiological ordering and serves as a baseline for evaluating agreement between instruments. Within each group, the paired gray connecting lines in Fig. 5 are generally short, indicating small per-subject differences. Mean paired differences (Colorimetric–Macroduct) are +3.5 mM in healthy, +1.3 mM in CRMS, +0.98 mM in CF with modulators, and −0.94 mM in CF without modulators. These biases are clinically negligible relative to the group means and dispersions. Paired *t*-tests across all groups are non-significant ($p > 0.40$–0.57), confirming that both systems provide statistically similar central tendencies within each subgroup. Variability increases with chloride concentration, with SDs of ~26–30 mM in CF groups and smaller SDs in healthy and CRMS participants, consistent with physiological heteroscedasticity. Mean absolute differences (MADs) between the two methods remain modest: ~4.3–4.6 mM for healthy, CRMS, and CF with modulators, and ~6.7 mM for CF without modulators. The slightly larger MAD at the upper chloride range likely reflects inherent biological variability rather than device drift. Supplementary Table 7 summarizes data of the paired comparison for these four groups.

Both instruments yielded the same, biologically coherent group ordering: healthy < CRMS < CF on modulators < CF off modulators. Chloride levels were significantly lower in CF participants on modulators than in those off therapy for both Macroduct ($p = 0.0002$) and CF SWIFT ($p = 0.0007$). Dispersion was modestly higher in the highest-chloride group (CF off modulators) for both systems, and the mean paired differences between the two methods showed no systematic bias across groups.

Discussion

Our findings demonstrate important advantages of the CF SWIFT technology over existing clinical sweat-testing systems. First, the soft, flexible mechanical designs of the stimulator and analyzer modules conform naturally to curved, mobile skin surfaces, bonded with medical-grade adhesives. This coupling reduces instances of motion-induced delamination, minimizes the potential for leakage at the skin interface, and avoids discomfort issues that are especially relevant in neonatal and pediatric CF

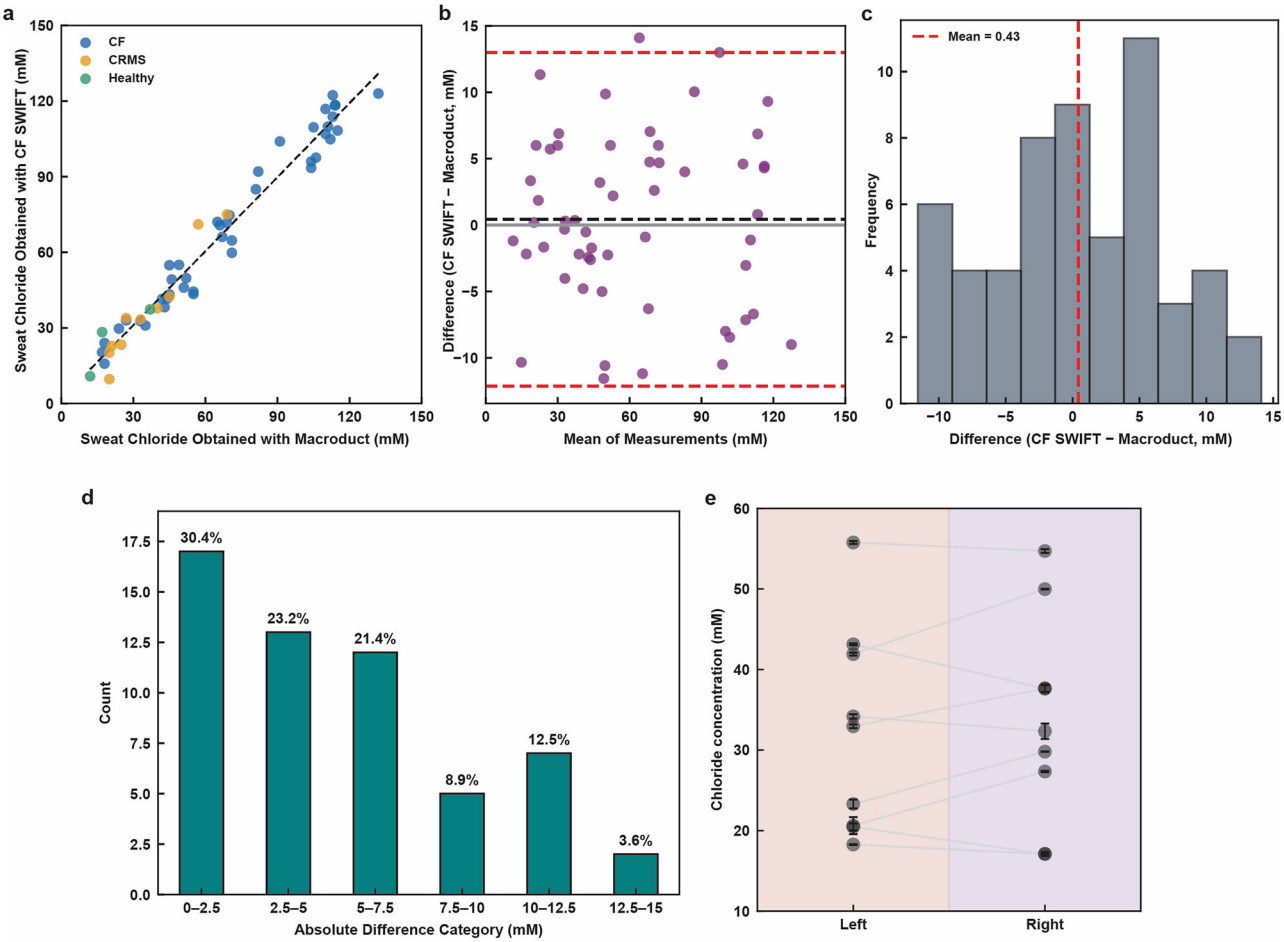
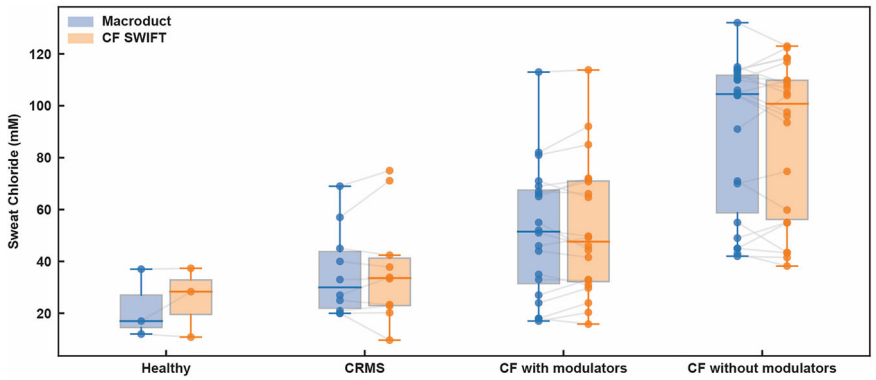


Fig. 4 | Clinical study device agreement. a Correlation between the Macroduct results and the CF SWIFT results. **b** Bland–Altman plot of the comparison study. **c** Distribution of paired differences of the comparison study. **d** Distribution of paired absolute differences. **e** Paired comparison of chloride results obtained by the CF SWIFT devices collected from the same human subject on contralateral arms; light gray lines connecting each subject's pair.

Fig. 5 | Distribution of Macroduct and SWIFT results for different groups of the study; light gray lines connecting each subject's pair.



testing. These features are in contrast with the tight circumferential strapping required for the rigid stimulation and collection apparatus being used currently as the standard of care.

Second, CF SWIFT reduces reliance on benchtop analytical instrumentation after sweat collection. Quantitative clinical validation in this study used controlled imaging (light box and digital camera) to limit illumination-related variance and to ensure a rigorous comparison to the reference method; the same workflow is nevertheless suited to smartphone acquisition in less controlled environments, as established in prior work[37,45,46] and consistent with the imaging experiments summarized in the Results. For CF SWIFT specifically, smartphone-based capture is attractive because it preserves an integrated, bedside-to-home workflow while remaining compatible with decentralized testing outside traditional sweat laboratories.

Third, the CF SWIFT system significantly reduces the volume of sweat needed for analysis. Conventional approaches require ≥ 15 µL of collected sweat, subsequently diluted into ~10 mL of working solution for instrumental analysis, consisting of specific concentrations of acid buffer and gelatin[43,47,48]. In contrast, each reservoir in the analyzer patch requires only 1.5 µL, including the volume to fill the microfluidic channels and the dead

volume held by the opening of the adhesive and inlet, to yield an accurate chloride measurement, corresponding to more than an order of magnitude reduction in required sweat and nearly three orders of magnitude less overall liquid for analysis using the current analytical workflow and instrumentation. This minimal volume requirement reduces reliance on larger volumes required in current standard-of-care testing while also potentially reducing the frequency of QNS outcomes.

Finally, the CF SWIFT system offers substantial cost advantages. Conventional sweat-testing infrastructure demands significant investments in equipment, personnel, and single-use components from supply kits. In contrast, manufacturing cost estimates for the CF SWIFT system indicate a much lower per-test cost. The reusable pilocarpine stimulation module consists of a simple miniaturized circuit and battery and is estimated to cost approximately $15 per unit. Each circuit supports approximately 30 stimulations, reducing the cost per test to well below one dollar. Roll-to-roll fabrication of the single-use colorimetric sweat collection and sensing patch is estimated at approximately $2 per unit at production volumes of ~250,000 units, with projected reductions to $1–1.25 per patch at higher volumes (≥500,000 units), consistent with prior reports of low-cost roll-to-roll processing strategies established for similar microfluidic patches[49,50]. The remaining single-use components, including pilocarpine-based hydrogels, are expected to contribute modestly to overall cost. Taken together, the total cost per test is projected to be on the order of one dollar (Supplementary Table 8). This cost structure creates opportunities for economically viable deployments in remote settings and in LMICs where access to traditional sweat-testing equipment remains severely constrained.

Collectively, these advantages can support clinical decision-making and patient care in several ways. The portability and low cost may enable confirmatory sweat testing in settings without centralized CF centers, potentially reducing delays after positive newborn screening. This reported study had no QNS tests with either the Macroduct or CF SWIFT platform, which may reflect the clinical proficiency of the research coordinators. The results therefore provide no basis to compare the performance of the two devices in this regard. Although CF SWIFT requires significantly less sweat than the Macroduct system, the potential for improved performance can only be evaluated in a large multisite study. The integrated collection-and-analysis workflow may shorten time-to-result and reduce dependence on trained operators, supporting earlier treatment decisions and monitoring of CFTR modulator response in resource-limited or remote settings.

Clinical data reported in this study indicate that limitations in the accuracy and precision of measurements of chloride concentration are primarily physiological, rather than instrumental, factors, consistent in magnitude with variations that can occur between contralateral arms. These results have also informed practical considerations that could minimize variability and maximize measurement yield. Excessive patient motion during the tests can, in certain cases, lead to partial delamination from the skin. A reinforcing bandage, positioned over the analyzer, can provide mechanical support and reduce this issue. Delays in image capture beyond ~30 min after sweat collection and chloranilate reaction can lead to evaporative effects in the reservoirs due to the permeability of PDMS. In the present work, completion of image capturing within 30 min of sweat collection ensured control of the evaporation effect. Although not adopted here, a thin, flexible polymeric overlay (e.g., PET), as employed in other studies[51], can substantially reduce sweat evaporation to levels negligible in real-world scenarios, and could be incorporated in future implementations if longer delays before image capture are required.

Limitations of the study include that sample sizes are limited for Healthy ($N = 3$) and, to a lesser extent, CRMS ($N = 10$) participants. As a result, the confidence intervals around means and biases in these groups were wider than expected. At the same time, the overall cohort still contained a wide sweat-chloride range, including near-normal and intermediate values, through participants who had CRMS and CF, notably those on CFTR modulators with lower sweat chloride. That composition supports assessment of device performance across much of the diagnostically relevant chloride spectrum, even though it does not substitute for a more numerous unselected healthy reference group. Furthermore, few infants < 1 year old were tested in this study, despite this age group being the most likely to benefit from a small, flexible device for CF diagnosis, as this present study was conducted at a single center that sees 10–12 infants per year with newly diagnosed CF; recruitment focused on the available clinic population as the primary goal was system validation. No QNS outcomes were observed in this study (0/55 participants). The primary aim was to evaluate agreement between the CF SWIFT and Macroduct systems for sweat chloride measurement; comparison of collection success or QNS rates between the two systems was not a primary objective and would require work with a population with a broader range of collection success rates. Validation in neonates and young infants, the group with the highest QNS rates with conventional methods, remains a priority that will be addressed in multi-clinical-site studies in future work.

Compared with the Macroduct standard-of-care device, several areas require improvement for the CF SWIFT platform. The Macroduct system has been validated across all pediatric age groups, including neonates, whereas the current study enrolled only two subjects under 12 months of age and none under 1 month; validation in this demographic is a priority. The Macroduct's rigid collector is less sensitive to motion-related detachment; the SWIFT platform may require a reinforcing bandage in high-motion settings. The Macroduct workflow does not impose a time limit on sample analysis, whereas SWIFT requires image capture within ~30 min to avoid evaporative effects. Finally, the Macroduct system benefits from established guidelines and extensive clinical evidence; the CF SWIFT platform will need larger, more diverse cohorts and guideline adoption to achieve comparable standing in clinical practice.

In summary, the CF SWIFT system demonstrates strong agreement with the Macroduct reference in a single-center cohort of 55 participants, with a higher proportion of individuals diagnosed with CF and smaller groups of CRMS and healthy controls. The parallel behavior observed in subgroup analysis demonstrates that this system tracks clinically meaningful inter-group differences comparably to the Macroduct standard. The platform offers a miniaturized, integrated alternative for sweat chloride measurement with potential to expand access to CF diagnosis and monitoring. Further development of this system has great potential to improve availability of sweat testing to underserved populations in high-resource countries and to expand sweat testing to LMICs where CF diagnostic testing is largely unavailable. Further, since sweat chloride is the most important pharmacodynamic marker of therapies that improve CFTR function, this "laboratory-free" measurement system can support distributed and remote clinical trials of new therapies. Finally, frequent and remote sweat monitoring may be useful in monitoring disease status and effects of therapies in people with CF[37]. Validation studies spanning multiple clinical sites and remote home testing in neonates and young infants, and in broader populations, will be important next steps to establish its role in clinical practice.

Methods

Fabrication of the circuit, hydrogel, and microfluidic device

Certain overall design features of the stimulation module reported here relied on adapted versions of those previously published[36]. Briefly, Autodesk Fusion facilitated design of the fPCB with size 57 × 10 mm, manufactured by an ISO 9001-compliant vendor. By folding the BLE chip pad over the anode pad, the final PCB footprint within the silicone encapsulation was reduced to 43 × 10 mm. The stimulation pads (anode and cathode) each have sizes of 13.5 × 10 mm. Bonding of SMD circuit components to the fPCB used In/Ag solder paste applied with a heat gun. Supplementary Table 8 demonstrates a complete list of components and component cost. Marine epoxy coated onto the circuit board served as a water barrier. The pilocarpine-containing hydrogels used a 4% agarose

hydrogel containing 0.5 wt% pilocarpine nitrate formed by casting into silicone molds with recessed features in the required geometry (13.5 × 10 × 3 mm). The current limiting design and benchtop evaluation of electrical safety against IEC60601-1[52] ensured participant safety (Supplementary Note 1).

Fabrication of the analyzer patch began with spin-coating a layer of photoresist (KMPR 1010; MicroChem) onto a 1 mm-thick silicon wafer (4 inches in diameter) at 2000 rpm for 30 s. After pre-baking on a hot plate at 100 °C for 5 min, the wafer was exposed to ultraviolet light through a pre-patterned 5-inch Cr photomask. A subsequent post-exposure baking on a hot plate at 100 °C for 5 min, followed by immersion in developer (AZ 917MIF, Integrated Micro Materials) for 7 min, defined patterns for the collection channels, bursting valves, and sensing reservoirs, serving as the etching mask for the deep reactive ion etching (STS Pegasus ICP-DRIE, SPTS Technologies) process. A profilometer (Dektak-8, Veeco) measured a silicon etching rate and confirmed an etching depth of 200 ± 5 µm. Spin-coating and baking a layer of polymethylmethacrylate (PMMA; 3000 rpm for 30 s and 180 °C for 2 min) on the patterned silicon mold facilitated release of PDMS (Sylgard 184, Dow Corning; mixing ratio of base to curing agent of 10:1) thermal cured on top. Specifically, spin-coating of a PDMS precursor at 200 rpm for 30 s, followed by degassing under vacuum, and baking on a hot plate at 75 °C for 1 h, yielded a PDMS replica, featuring sweat collection and sensing channels. A mechanical biopsy punch with a diameter of 1.5 mm defined the two inlet holes. The colorimetric chloride assay consisted of 100 mg of silver chloranilate (MP Biomedicals, CA, USA) dispersed in 400 µL of 2 wt% polyhydroxyethylmethacrylate (pHEMA, Sigma-Aldrich, MO, USA) methanolic suspension, drop-cast (0.75 µL) in each of the two reservoirs. Leaving the patch with the drop-cast assay in a vacuum desiccator for 30 min at room temperature formed the dried assays in the reservoirs. Spin-coating a prepolymer to PDMS (10:1) onto a blank silicon wafer at 400 rpm for 30 s and curing at 75 °C for 1 h produced a 100 µm cover layer for the reservoirs and the entire microfluidic structure. Exposing this layer and the microfluidic layer to a corona discharge activated the surfaces to allow strong bonding between them upon contact. A mechanical die cutter defined the outer perimeter of the device and openings for the two hydrogel elements. A laser cutter (Universal Laser Systems, AZ, USA) defined patterns of dual-sided medical-grade adhesives (2477P, 3 M for the stimulation module, and 1524A, 3 M for the analyzer module) based on designs created in AutoCAD. Bonding to the microfluidic platform relied on contact after a corona treatment.

Encapsulation of the stimulation circuit began with the design of complementary convex and concave aluminum molds in SOLIDWORKS 2023, followed by production of the molds with a milling machine (MDX-540, Roland DGA). A silicone layer (Silbione RTV-4410, mixed with 5 wt% white silicone dye) cast against these molds and thermally cured at 70 °C for 30 min formed the top encapsulation layer. Marine epoxy (3 M Marine Adhesive Sealant) sealed the electronic circuit components as a water barrier. A fast-curing elastomer (Ecoflex 00-35), which solidifies in 10 min, embedded the circuit within the encapsulation structure.

CF SWIFT stimulation circuit characterization

Output stimulation current was measured with a 5½-digit digital multimeter (DM3058E, RIGOL) during single-fault testing (Supplementary Note 1) and immediately before and after cyclic bending fatigue testing. Power consumption measurements used a Nordic Semiconductor Power Profiler Kit II (PPK2) operated in source meter mode at a fixed supply voltage of 4.0 V, with current logged at 100 samples per second (10 ms sampling interval) for recordings of five devices and triplicate measurements per device.

Finite element analysis

The electromagnetic simulation of the electric field generated by electrodes inside the skin used the commercial software, Ansys Maxwell. The bulk conductivity (σ) was 0.1 S·m^{-1} for the skin. The simulation applied a current of 0.25 mA to the electrodes, matching the fixed current level in on-human studies. Adoption of an adaptive mesh (tetrahedron elements) ensured computational accuracy.

The mechanical simulations used the commercial software ABAQUS to study the mechanical response of the device mounted on skin, including stretching, bending, and twisting. The mesh convergence was guaranteed for all cases, and the mesh was refined in the serpentine area. Four-node composite shell elements were used for the polyimide (PI) layers and copper traces, and eight-node solid elements were used for the skin part. PI was modeled as a linear elastic material with an elastic modulus of 2.5 GPa and Poisson's ratio of 0.34. Copper was modeled as a linear elastic material with an elastic modulus of 110 GPa and Poisson's ratio of 0.35. During stretching, displacements corresponding to 15% stretching were applied to the ends of the skin part. During bending, the bottom surface of the skin part was pressed against a rigid cylinder with a 50 mm radius. During twisting, the two ends of the skin phantom were twisted by approximately 90°. The strain distributions were output for each layer with different types of loading.

Development and characterization of the colorimetric chloride assay

A UV-vis spectrophotometer (NanoDrop 2000; Thermo Fisher Scientific, MA, USA) recorded the absorbance spectra of the assays after exposure to chloride solutions with varying concentrations. Taking images of the microfluidic reservoirs filled with aqueous solutions of chloride at concentrations from 0 mM to 120 mM followed by image-based colorimetric analysis, yielded calibration curves. Preparation of artificial sweat solutions (Artificial Eccrine Perspiration, Pickering Test Solutions) spanning the clinically relevant chloride range enabled quantification by ICP-OES. Measurement of each concentration in quadruplicate using the SWIFT patch led to agreement evaluation using comparison of expected vs measured chroma and Bland–Altman analysis of derived chloride concentration.

Image-based colorimetric analysis

The setup for colorimetric analysis relied on images captured in a light box (Godox LSD80 Light Tent, China) using a digital camera (Canon EOS 6D, Japan) with an X-rite ColorChecker (X-rite, MI, USA) in the field of view as a color reference. A Python-based algorithm processed the captured images (Supplementary Fig. 2)[53]. The analysis software extracted color information from six manually defined regions of interest (ROIs) within each reservoir, excluding shadowed areas and structural defects. After baseline calibration of color intensity and temperature using the ColorChecker, the algorithm computed the average and standard deviation of L*, a*, b*, and chroma (C*) values in the CIELAB color space. Smartphone imaging under varied lighting used the same analyzer patches ($n = 4$) photographed with an iPhone 16 and a digital camera under four conditions ranging from 500 lux to 10,000 lux, analyzed with the same colorimetric pipeline as for clinical images.

Bilateral testing with laboratory ground truth

The in-lab bilateral testing in healthy subjects using the CF SWIFT system involved nine adult volunteers (aged 21–32), all of whom provided informed consent prior to participation. The test operator cleaned the skin of the forearm on each participant with an alcohol gauze pad, rinsed with deionized water, and dried with a clean tissue before attachment of the device. Testing used the CF SWIFT system on contralateral arms. Chloride concentrations determined by inductively coupled plasma mass spectrometry (ICP-MS; iCap 7600, Thermo Fisher Scientific, MA, USA) served as the ground truth.

Clinical study

The protocol was approved by the Institutional Review Board of Ann & Robert H. Lurie Children's Hospital of Chicago (IRB #2018–1440, clinical trial number: not applicable). Participants with CF, Cystic Fibrosis Related Metabolic Syndrome (CRMS), and healthy volunteers were recruited

between May 2022 and July 2025 from Ann & Robert H. Lurie Children's Hospital of Chicago. Participants or their legally authorized guardians provided written informed consent. The study used a bilateral sweat-testing design to compare the Macroduct system with the CF SWIFT platform. Additional details of the study design, including cohort characteristics, recruitment, and the bilateral comparison protocol, are provided in the Results section.

Data collection

The study team collected and managed data using Research Electronic Data Capture (REDCap) tools hosted by Northwestern University. REDCap helped enable reliable, compliant, and efficient management of clinical study data.

Statistical analysis

The analysis used Python (version 3.10.9) with standard scientific libraries including NumPy, SciPy, pandas, and statsmodels. The workflow summarized data as mean ± standard deviation unless noted otherwise. The analysis compared different experimental groups and evaluated demographic variables and survey results using appropriate statistical tests based on data type and distribution. Linear regression evaluated relationships between measurement conditions. Pearson correlation coefficients (r) quantified the association between results from the clinical standard and the proposed platform. Bland–Altman analysis assessed agreement between paired measurements from the Macroduct Advanced System and the CF SWIFT. For each device group, testing of overall differences across the four groups (Healthy, CRMS, CF with modulators, CF without modulators) used one-way ANOVA (parametric) and, to relax distributional assumptions, Kruskal-Wallis (nonparametric), both two-sided with $\alpha = 0.05$. When overall tests indicated heterogeneity, pairwise comparisons using Tukey's HSD (familywise error control) and also Mann-Whitney U tests with Holm correction enabled nonparametric sensitivity analysis.

Data availability

The datasets generated and/or analyzed in this current study are not publicly available due to the inclusion of human clinical data with potential risk of subject re-identification, but are available from the corresponding author on reasonable request. The underlying code for this study is available on GitHub and can be accessed via this link (https://github.com/EpicoreBiosystems/CF_Patch_Chloride_Analysis).

Code availability

The underlying code for this study is available on GitHub and can be accessed via this link.

Received: 4 February 2026; Accepted: 20 July 2026;
Published online: 28 July 2026

References

1. Brasier, N. et al. Applied body-fluid analysis by wearable devices. *Nature* **636**, 57–68 (2024).
2. Wu, Z. et al. Interstitial fluid-based wearable biosensors for minimally invasive healthcare and biomedical applications. *Commun. Mater.* **5**, 33 (2024).
3. Wang, K. et al. Smart wearable sensor fuels noninvasive body fluid analysis. *ACS Appl. Mater. Interfaces* **17**, 13279–13301 (2025).
4. Santos, T. F., Galvão, F. M. F., Neto, L. O. & Nascimento, J. H. O. Emerging technologies in wearable sweat sensors for next-generation real-time health monitoring. *ACS Mater. Lett.* **7**, 3341–3362 (2025).
5. Bordin, D. M., McCauley, J. I., Campos, E. G. d., Bishop, D. P. & Martinis, B. S. D. Sweat as a diagnostic biofluid: analytical advances and future directions. *J. Pharmaceut. Anal.* **16**, 101473 (2025).
6. Yang, D. S., Ghaffari, R. & Rogers, J. A. Sweat as a diagnostic biofluid. *Science* **379**, 760–761 (2023).
7. Liu, W. et al. Skin-interfaced colorimetric microfluidic devices for on-demand sweat analysis. *npj Flexible Electron.* **7**, 43 (2023).
8. Li, F. et al. Flexible wearable microfluidic colorimetric sensor for multiplex bioenzyme-free detection of creatinine, urea, and magnesium ions in sweat. *ACS Appl. Mater. Interfaces* **17**, 36444–36454 (2025).
9. R. et al. Worth your sweat: wearable microfluidic flow rate sensors for meaningful sweat analytics. *Lab Chip* **25**, 1296–1315 (2025).
10. Ha, J.-H. et al. A wearable colorimetric sweat pH sensor-based smart textile for health state diagnosis. *Mater. Horiz.* **10**, 4163-4171 (2023).
11. Yang, D. S. et al. Soft, skin-interfaced 3D microfluidic systems for high performance assessment of sweat rate, cumulative loss and biochemical content. *Adv. Funct. Mater.* **36**, e09169 (2026).
12. Gibson, L. E. & Cooke, R. E. A test for concentration of electrolytes in sweat in cystic fibrosis of the pancreas utilizing pilocarpine by iontophoresis. *Pediatrics* **23**, 545–549 (1959).
13. Rosenstein, B. J., Langbaum, T. S., Gordes, E. & Brusilow, S. W. Cystic fibrosis: problems encountered with sweat testing. *JAMA* **240**, 1987–1988 (1978).
14. Clinical and Laboratory Standards Institute. *Newborn Screening for Cystic Fibrosis*, 2nd edn CLSI NBS05 (Clinical and Laboratory Standards Institute, 2019).
15. Farrell, P. M. et al. Diagnosis of cystic fibrosis: consensus guidelines from the cystic fibrosis foundation. *J. Pediatr.* **ume 181**, S4–S15.e11 (2017).
16. Gokdemir, Y. & Karadag, B. T. Frontiers|sweat testing and recent advances. *Front. Pediatr.* **9**, 649904 (2021).
17. Zemanick, E. T. et al. Sweat chloride reflects CFTR function and correlates with clinical outcomes following CFTR modulator treatment. *J. Cyst. Fibros.* **24**, 246–254 (2025).
18. Raina, M. A. et al. Assessment of correlation between sweat chloride levels and clinical features of cystic fibrosis patients. *J. Clin. Diagn. Res.* **10**, BC01–BC06 (2016).
19. Macedo, A. N. et al. The sweat metabolome of screen-positive cystic fibrosis infants: revealing mechanisms beyond impaired chloride transport. *ACS Central Sci.* **3**, 904–913 (2017).
20. Burgel, P.-R. et al. Sweat chloride and lung function responses to elexacaftor–tezacaftor–ivacaftor in people with cystic fibrosis with two versus one responsive CFTR variants: an analysis of two real-world observational studies. *Lancet Respir Med* **13**, 978–989 (2025).
21. McColley, S. A. et al. Quantity not sufficient rates and delays in sweat testing in US infants with cystic fibrosis. *Pediatr. Pulmonol.* **55**, 3053–3056 (2020).
22. Cirilli, N. et al. Real life practice of sweat testing in Europe. *J. Cyst. Fibros.* **27**, S1569-1993(17)30881-0 (2017).
23. Emaminejad, S. et al. Autonomous sweat extraction and analysis applied to cystic fibrosis and glucose monitoring using a fully integrated wearable platform. *Proc. Natl. Acad. Sci. USA* **114**, 4625–4630 (2017).
24. Rueegg, C. S. et al. Comparison of two sweat test systems for the diagnosis of cystic fibrosis in newborns. *Pediatr. Pulmonol.* **54**, 264–272 (2019).
25. Langen, A.V.-v. et al. Clinical evaluation of the Nanoduct sweat test system in the diagnosis of cystic fibrosis after newborn screening. *Eur. J. Pediatr.* **174**, 1025–1034 (2015).
26. Roberts, J. M., Wilcox, P. G. & Quon, B. S. Evaluating adult cystic fibrosis care in BC: disparities in access to a multidisciplinary treatment centre. *Can. Respir. J.* **2016**, 8901756 (2016).
27. DiMango, E. et al. Health disparities among adults cared for at an urban cystic fibrosis program. *Orphanet J. Rare Dis.* **16**, 332 (2021).
28. Heffernan, M. E. et al. The newborn screening experience of caregivers of children with cystic fibrosis in the United States: a cross-sectional survey. *Pediatr. Pulmonol.* **60**, e71110 (2025).

29. McColley, S., Roldan, M., Elbert, A. & Wu, R. *Cystic Fibrosis National Indicator Report 2024* (Lurie Children's Hospital, 2024).
30. Leung, D. H. et al. Effects of diagnosis by newborn screening for cystic fibrosis on weight and length in the first year of life. *JAMA Pediatr.* 171, 546–554 (2017).
31. Martiniano, S. L. et al. Late diagnosis in the era of universal newborn screening negatively affects short- and long-term growth and health outcomes in infants with cystic fibrosis. *J. Pediatr.* **262**, 113595 (2023).
32. Marks, M. P. et al. Most short children with cystic fibrosis do not catch up by adulthood. *Nutrients* **13**, 13 (2021).
33. Guo, J., Garratt A. & Hill A. Worldwide rates of diagnosis and effective treatment for cystic fibrosis. *J. Cystic Fibros* **21**, 456–462 (2022).
34. Varkki, S. D. et al. CFTR mutations and phenotypic correlations in people with cystic fibrosis: a retrospective study from a single centre in south India. *Lancet Reg Health Southeast Asia* **27**, 100434 (2024).
35. Farrell, P. M., Paul, G. R. & Varkki, S. D. India: the last and best frontier for cystic fibrosis newborn screening with perspectives on special challenges. *Int. J. Neonatal Screen.* **11**, 27 (2025).
36. Kim, J. et al. A skin-interfaced, miniaturized platform for triggered induction, capture and colorimetric multicomponent analysis of microliter volumes of sweat. *Biosens. Bioelectron.* **253**, 116166 (2024).
37. Nelson, R. S. et al. Remote analysis and management of sweat biomarkers using a wearable microfluidic sticker in adult cystic fibrosis patients. *Proc. Natl. Acad. Sci. USA* **122**, e2506137122 (2025).
38. Kim, C. & Kim, C. H. Universal testing apparatus implementing various repetitive mechanical deformations to evaluate the reliability of flexible electronic devices. *Micromachines (Basel)* **9**, 492 (2018).
39. Qaiser, N., Suryaprabha, T., Vetrano, F., Hwang, B. & Elatab, N. Mechanics and bio-interface engineering in flexible biosensors for continuous health monitoring. *npj Flexible Electron.* **10**, 23 (2026).
40. Ray, T. R. et al. Soft, skin-interfaced sweat stickers for cystic fibrosis diagnosis and management. *Sci. Transl. Med.* **13**, eabd8109 (2021).
41. Green, D. M. et al. Cystic fibrosis foundation evidence-based guideline for the management of CRMS/CFSPID open access. *Pediatrics* **153**, e2023064657 (2024).
42. LeGrys, V. A., Moon, T. C., Laux, J., Accurso, F. & Martiniano, S. A. A multicenter evaluation of sweat chloride concentration and variation in infants with cystic fibrosis. *J. Cyst. Fibros.* **18**, 190–193 (2019).
43. Foundation, C. F. *Sweat Test Clinical Care Guidelines* (Cystic Fibrosis Foundation, 2017).
44. Massie, J. et al. Australasian guideline (2nd edition): an annex to the CLSI and UK guidelines for the performance of the sweat test for the diagnosis of cystic fibrosis. *Clin. Biochem. Rev.* **38**, 115–130 (2017).
45. Choi, J. et al. Soft, skin-integrated multifunctional microfluidic systems for accurate colorimetric analysis of sweat biomarkers and temperature. *ACS Sens.* **4**, 379–388 (2019).
46. Yang, D. S. et al. Soft, skin-interfaced 3D microfluidic systems for high performance assessment of sweat rate, cumulative loss and biochemical content. *Adv. Functl. Mater.* **36**, e09169 (2026).
47. Choi, D.-H. et al. Sweat test for cystic fibrosis: wearable sweat sensor vs. standard laboratory test. *J. Cyst. Fibros.* **17**, 35–38 (2018).
48. ELITechGroup Inc. *Laboratory Procedure for the ChloroChek® Chloridometer* (ELITechGroup, 2014).
49. Baker, L. B. et al. Skin-interfaced microfluidic system with personalized sweating rate and sweat chloride analytics for sports science applications. *Sci. Adv.* **6**, eabe3929 (2020).
50. Ghaffari, R. et al. The Gx Sweat Patch for personalized hydration management. *Nat. Rev. Bioeng*. **1**, 5–7 (2023).
51. Cho, S. et al. Wearable lateral flow assays for cortisol monitoring with time-dynamic sweat sampling and sensing by electrochromic timers. *Nat. Sensors* **1**, 11 (2026).
52. International Electrotechnical Commission. Medical electrical equipment – Part 1: General requirements for basic safety and essential performance. International Electrotechnical Commission: Geneva; 2020.
53. Baker, L. B. et al. Skin-interfaced microfluidic system with machine learning-enabled image processing of sweat biomarkers in remote settings. *Adv. Mater. Technol*. **7**, 2200249 (2022).

Acknowledgements

This work made use of the Keck II facility, supported by the NCI Cancer Center Support Grant #P30 CA060553, and the NUFAB facility (RRID: SCR_017779) of Northwestern University's NUANCE Center, which has received support from the SHyNE Resource (NSF ECCS_2025633), the IIN, and Northwestern's MRSEC program (NSF FMR_2308691). This work was supported by the National Research Foundation of Korea(NRF) grant funded by the Korea government(MSIT) (RS-2025-24873030). Clinical research personnel and infrastructure was provided by the Stanley Manne Children's Research Institute, Division of Pulmonary and Sleep Medicine, Ann & Robert H. Lurie Children's Hospital of Chicago.

Author contributions

M.Z., D.S.Y., and Joohee.K. contributed equally to this work and are considered co-first authors. Conception, design, and study direction: J.A.R., S.A.M., R.G., M.Z., D.S.Y., and Joohee.K. Device design, prototype and fabrication: M.Z., D.S.Y., Joohee.K., J.-H.K., E.E.K., J.U.K., S.O., S.L., S.K., Jiheon.K., H.H., J.P., T.Z., C.P., S.G.S., Y.J., J.C., Jiwon.K., and Y.H. Clinical experiments and data acquisition: M.Z., D.S.Y., J.K., E.E.K., and L.R. Data analysis: M.Z., D.S.Y., J.K., T.Z., and A.J.A. Manuscript writing and review: M.Z., M.J., R.G., S.A.M, and J.A.R. All authors have read and approved the manuscript.

Competing interests

A.J. Aranyosi, R. Ghaffari and J.A. Rogers are affiliated with Epicore Biosystems, which develops and commercializes microfluidic devices for sweat analysis. M. Jain is a clinical advisor to Epicore Biosystems, for which he receives no fees. S.A. McColley is a clinical advisor to Epicore Biosystems, for which she receives no fees; and an advisor to Vertex Pharmaceuticals, Inc., for which she receives fees. CF SWIFT is not owned by Epicore Biosystems. Epicore Biosystems may seek to access the technology and associated intellectual property through the Northwestern University technology transfer office in the future. Author J.A. Rogers is Associate Editor of npj Digital Medicine. J.A. Rogers was not involved in the journal's review of, or decisions related to, this manuscript. All other authors declare no competing interests.

Additional information

Supplementary information The online version contains supplementary material available at https://doi.org/10.1038/s41746-026-03056-9.

Correspondence and requests for materials should be addressed to Susanna A. McColley or John A. Rogers.

Reprints and permissions information is available at http://www.nature.com/reprints

Publisher's note Springer Nature remains neutral with regard to jurisdictional claims in published maps and institutional affiliations.

Open Access This article is licensed under a Creative Commons Attribution-NonCommercial-NoDerivatives 4.0 International License, which permits any non-commercial use, sharing, distribution and reproduction in any medium or format, as long as you give appropriate credit to the original author(s) and the source, provide a link to the Creative Commons licence, and indicate if you modified the licensed material. You do not have permission under this licence to share adapted material derived from this article or parts of it. The images or other third party material in this article are included in the article's Creative Commons licence, unless indicated otherwise in a credit line to the material. If material is not included in the article's Creative Commons licence and your intended use is not permitted by statutory regulation or exceeds the permitted use, you will need to obtain permission directly from the copyright holder. To view a copy of this licence, visit http://creativecommons.org/licenses/by-nc-nd/4.0/.

© The Author(s) 2026

[1]Querrey Simpson Institute for Bioelectronics, Northwestern University, Evanston, IL, USA. [2]Department of Biomedical Engineering, Northwestern University, Evanston, IL, USA. [3]School of Mechanical Engineering, Chung-Ang University, Seoul, Republic of Korea. [4]Center for Bionics of Biomedical Research Institute, Korea Institute of Science and Technology, Seoul, Republic of Korea. [5]Department of Mechanical Engineering, Massachusetts Institute of Technology, Cambridge, MA, USA. [6]School of Chemical Engineering, Sungkyunkwan University (SKKU), Suwon, Republic of Korea. [7]Division of Electrical Engineering, Hanyang University ERICA, Ansan, Republic of Korea. [8]Stanley Manne Children's Research Institute, Ann & Robert H. Lurie Children's Hospital of Chicago, Chicago, IL, USA. [9]Department of Mechanical Engineering, Northwestern University, Evanston, IL, USA. [10]School of Electrical Engineering, Korea Advanced Institute of Science and Technology, Daejeon, Republic of Korea. [11]Department of Chemistry, Sejong University, Seoul, Republic of Korea. [12]Department of Materials Science and Engineering, Gwangju Institute of Science and Technology (GIST), Gwangju, Republic of Korea. [13]School of Chemical Engineering, Sungkyunkwan University, Seoul, Republic of Korea. [14]Epicore Biosystems Inc., Cambridge, MA, USA. [15]Division of Pulmonary and Critical Care Medicine, Feinberg School of Medicine, Northwestern University, Chicago, IL, USA. [16]Division of Pulmonary and Critical Care Medicine, Northwestern University, Chicago, IL, USA. [17]Jesse Brown VA Hospital, Chicago, IL, USA. [18]Simpson Querrey Lung Institute for Translational Science, Northwestern University, Chicago, IL, USA. [19]Division of Pulmonary and Sleep Medicine, Department of Pediatrics, Northwestern University Feinberg School of Medicine, Chicago, IL, USA. [20]Department of Materials Science and Engineering, Northwestern University, Evanston, IL, USA. [21]Department of Civil and Environmental Engineering, Northwestern University, Evanston, IL, USA. [22]These authors contributed equally: Mingyu Zhou, Da Som Yang, Joohee Kim.
✉e-mail: SMcColley@luriechildrens.org; jrogers@northwestern.edu